作成方法であるかは問題ではない。informal approachで専門家が熟慮の末に報告した項目をformal approachでconsensusが得られるか検討することが可能であったことは，先行研究者に深く感謝せずにはいられない。今後の研究結果によっては，実臨床に役立つ客観性をly，vにもたせることはできないかもしれないが，今回の手法が，しばしば指摘される病理判定における客観性の低さを解決するモデルとなれば，病理学や医学に貢献できる可能性があり，われわれにとっても幸いである。

References

1) Harris EI, Lewin DN, Wang HL, et al : Lymphovascular invasion in colorectal cancer : an interobserver variability study. *Am J Surg Pathol* **32** (12) : 1816-1821, 2008
2) 下田忠和，谷口浩和，池上雅博ほか：転移・予後因子としてのリンパ管・静脈侵襲程度の再評価．大腸疾患Now2010．杉原健一，藤盛孝博，五十嵐正広，ほか(編)，日本メディカルセンター，東京，pp.133-141，2010
3) キャサリン・ボーブ，ニコラス・メイズ(編)，大滝純司(監訳)：Delphi processやnominative groupによる保健・医療サービスの研究．質的研究実践ガイド．医学書院，東京，pp.44-53，2001
4) Klimstra DS, Modlin IR, Adsay NV, et al : Pathology reporting of neuroendocrine tumors : application of the Delphic consensus process to the development of a minimum pathology data set. *Am J Surg Pathol* **34** (3) :300-313, 2010

厚生労働科学研究費補助金

革新的がん医療実用化研究事業

「我が国で新しく発明された概念に基づく抗がん剤アルクチゲニン臨床第Ⅱ相試験による膵がん克服」に関する研究

平成24年度～平成26年度　総合研究報告書

研究代表者　　江角　浩安

平成27（2015）年　5月

平成25年度

研究成果の刊行物・別刷

Am J Physiol Cell Physiol 306: C320–C321, 2014;
doi:10.1152/ajpcell.00362.2013.

"S'ils n'ont pas de pain, qu'ils mangent de la brioche." Focus on "Anaerobic respiration sustains mitochondrial membrane potential in a prolyl hydroxylase pathway-activated cancer cell line in a hypoxic microenvironment"

Hiroyasu Esumi

Research Institute for Biomedical Sciences, Tokyo University of Science, Yamazaki, Noda, Chiba, Japan

IN THEIR ARTICLE, published in this issue of the *American Journal of Physiology-Cell Physiology*, Takahashi and Sato (7) point to the possibility that anaerobic respiration depends on complex II activity in mammalian cells, especially cancer cells. Fumarate respiration is established in parasites and shellfish but has not been unequivocally demonstrated in mammalian cells. What cancer cells are eating to generate energy for survival without oxygen and glucose is one challenging subject.

Cancer cells depend on glycolysis for their energy production, even during sufficient oxygen supply, and this dependence on glycolysis for energy production, i.e., the Warburg effect, has long been believed to be one of the most general characteristics of cancer (8). On the other hand, tumor angiogenesis is also strongly activated in most cancer tissues through activation of hypoxia-inducible factor (HIF)-1-dependent and -independent pathways, and tumor angiogenesis is often closely associated with poor prognosis for patients with various types of cancer (5). However, many clinical investigations have revealed that most cancer tissues are strongly hypoxic, despite vigorous angiogenesis and the preference of cancer cells for glycolysis. Therefore, cancer tissue hypoxia is assumed to be a result of insufficient blood supply. Tumor vasculature might be subjected to structural distortion by continuous tumor growth and death, resulting in structural and functional immaturity. The main energy production pathway of mammalian cells in an anaerobic environment is believed to be glycolysis, but, in the case of tumor hypoxia, glucose and other nutrient supplies might also be limited. Information about how cancer cells produce energy to maintain their proliferation and/or life under such harsh conditions is limited (2, 3).

Several authors have proposed the possibility of anaerobic respiration by renal cells and cancer cells, but its biochemical mechanisms and significance remain to be established (5, 6). Takahashi and Sato (7) used an elegant experimental system to demonstrate the possibility of an alternative anaerobic respiration. They developed a two-dimensional tissue model in which a monolayer of cultured cells expressing green fluorescent protein was placed under a coverslip so that oxygen is supplied only from the edge of the coverslip. In this system, an oxygen gradient was formed and visualized as the red shift of fluorescence, which depends on oxygen tension (6). When mitochondrial membrane potential was also visualized by a cationic fluorescent dye, the point at which the oxygen supply became limiting for mitochondrial function could be established. Using this system, they showed that the maximum distance for diffusion of oxygen was ~500 μm from the oxygen source (the edge of the coverslip), at which point mitochondrial membrane potential was abolished [the anoxic front (AF)]. When prolyl hydroxylase domain-containing proteins were inhibited by dimethyloxalylglycine (DMOG), the AF was extended to 1,500–2,000 μm, and the effect was much more prominent in a cancer cell line than in a fibroblast-like cell line. DMOG pretreatment significantly reduced tissue oxygen gradients, indicating sustained mitochondrial membrane potential with reduced respiration. In addition, DMOG effects were completely abolished by pharmacological inhibition of complex II, but not complex III, suggesting that complex II (probably with complex I) sustains mitochondrial membrane potential in the absence of oxygen (anaerobic respiration) in cells in which PHD activity is inhibited.

Recently, the importance of α-ketoglutarate-dependent dioxygenases in biology has been widely accepted, and this is especially true for the HIF-1 pathway in cancer and epigenetic regulation of cellular function. In the work of Takahashi and Sato (7), DMOG was used to activate hypoxic adaptation, and "cellular anaerobic respiration" was found to be activated. HIF-1 is the most important and well-studied transcription factor regulating a wide variety of cellular adaptations to the hypoxic environment. However, α-ketoglutarate-dependent dioxygenases include a large number of family members, and DMOG is not highly specific for the prolyl hydroxylases that regulate HIF-1α. The recent discovery of isocitrate dehydrogenase mutations, which produce large increases in the levels of the "onco-metabolite" D-2-hydroxyglutarate, raised the following question: How does this metabolite exert its oncogenic effect? HIF-1 activation is a strong candidate, but more extensive genetic and biochemical analyses, including effects on TET dioxygenases, histone demethylases, and prolyl hydroxylases, are needed to explore the biological relevance of D-2-hydroxyglutarate (1) and the work of Takahashi and Sato (7).

The work of Takahashi and Sato (7) points to the possibility that anaerobic respiration depends on complex II activity in mammalian cells, especially cancer cells, and this is one of the most interesting possibilities. Fumarate respiration is established in parasites and shellfish but has not been unequivocally demonstrated in mammalian cells (4). What cancer cells are eating to generate energy for survival without oxygen and glucose is one challenging subject. Additional genetic and biochemical studies are needed.

Address for reprint requests and other correspondence: H. Esumi, Research Institute for Biomedical Sciences, Tokyo Univ. of Science, 2669 Yamazaki, Noda, Chiba 278-0022, Japan (e-mail: hesumi@rs.tus.ac.jp).

DISCLOSURES

No conflicts of interest, financial or otherwise, are declared by the author.

AUTHOR CONTRIBUTIONS

H.E. drafted the manuscript; H.E. approved the final version of the manuscript.

REFERENCES

1. **Cairns RA, Mak TW.** Oncogenic isocitrate dehydrogenase mutations: mechanisms, models, and clinical opportunities. *Cancer Discov* 3: 730–741, 2013.
2. **DeBerardinis RJ, Lum JJ, Hatzivassiliou G, Thompson CB.** The biology of cancer: metabolic reprogramming fuels cell growth and proliferation. *Cell Metab* 7: 11–20, 2008.
3. **Esumi H, Izuishi K, Kato K, Hashimoto K, Kurashima Y, Kishimoto A, Ogura T, Ozawa T.** Hypoxia and nitric oxide treatment confer tolerance to glucose starvation in a 5′-AMP-activated protein kinase-dependent manner. *J Biol Chem* 277: 32791–32798, 2002.
4. **Sakai C, Tomitsuka E, Esumi H, Harada S, Kita K.** Mitochondrial fumarate reductase as a target of chemotherapy: from parasites to cancer cells. *Biochim Biophys Acta* 1820: 643–651, 2012.
5. **Semenza GL.** Regulation of metabolism by hypoxia-inducible factor 1. *Cold Spring Harb Symp Quant Biol* 76: 347–353, 2011.
6. **Takahashi E, Sato M.** Imaging of oxygen gradients in monolayer cultured cells using green fluorescent protein. *Am J Physiol Cell Physiol* 299: C1318–C1323, 2010.
7. **Takahashi E, Sato M.** Anaerobic respiration sustains mitochondrial membrane potential in a prolyl hydroxylase pathway-activated cancer cell line in a hypoxic microenvironment. *Am J Physiol Cell Physiol* (September 18, 2013). doi:10.1152/ajpcell.00255.2013.
8. **Warburg O.** On the origin of cancer cells. *Science* 123: 309–314, 1956.

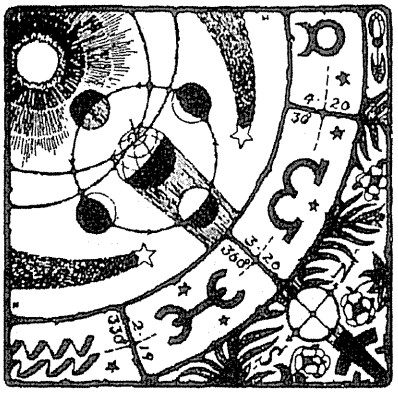

Metabolomics (2013) 9:444–453
DOI 10.1007/s11306-012-0452-2

ORIGINAL ARTICLE

Metabolomic profiling of lung and prostate tumor tissues by capillary electrophoresis time-of-flight mass spectrometry

Kenjiro Kami · Tamaki Fujimori · Hajime Sato · Mutsuko Sato · Hiroyuki Yamamoto · Yoshiaki Ohashi · Naoyuki Sugiyama · Yasushi Ishihama · Hiroko Onozuka · Atsushi Ochiai · Hiroyasu Esumi · Tomoyoshi Soga · Masaru Tomita

Received: 11 June 2012 / Accepted: 27 July 2012 / Published online: 2 November 2012

Abstract Metabolic microenvironment of tumor cells is influenced by oncogenic signaling and tissue-specific metabolic demands, blood supply, and enzyme expression. To elucidate tumor-specific metabolism, we compared the metabolomics of normal and tumor tissues surgically resected pairwise from nine lung and seven prostate cancer patients, using capillary electrophoresis time-of-flight mass spectrometry (CE-TOFMS). Phosphorylation levels of enzymes involved in central carbon metabolism were also quantified. Metabolomic profiles of lung and prostate tissues comprised 114 and 86 metabolites, respectively, and the profiles not only well distinguished tumor from normal tissues, but also squamous cell carcinoma from the other tumor types in lung cancer and poorly differentiated tumors from moderately differentiated tumors in prostate cancer. Concentrations of most amino acids, especially branched-chain amino acids, were significantly higher in tumor tissues, independent of organ type, but of essential amino acids were particularly higher in poorly differentiated than moderately differentiated prostate cancers. Organ-dependent differences were prominent at the levels of glycolytic and tricarboxylic acid cycle intermediates and associated energy status. Significantly high lactate concentrations and elevated activating phosphorylation levels of phosphofructokinase and pyruvate kinase in lung tumors confirmed hyperactive glycolysis. We highlighted the potential of CE-TOFMS-based metabolomics combined with phosphorylated enzyme analysis for understanding tissue-specific tumor microenvironments, which may lead to the development of more effective and specific anticancer therapeutics.

Keywords Metabolomics · CE-MS · Phosphoproteomics · Lung cancer · Prostate cancer · Tumor microenvironment

Kenjiro Kami and Tamaki Fujimori contributed equally to this study.

Electronic supplementary material The online version of this article (doi:10.1007/s11306-012-0452-2) contains supplementary material, which is available to authorized users.

K. Kami · Y. Ohashi · N. Sugiyama · T. Soga · M. Tomita
Institute for Advanced Biosciences, Keio University, Tsuruoka, Yamagata, Japan

K. Kami · T. Soga · M. Tomita
Systems Biology Program, Graduate School of Media and Governance, Keio University, Fujisawa, Kanagawa, Japan

T. Fujimori · H. Sato · M. Sato · H. Yamamoto · Y. Ohashi (✉) · T. Soga · M. Tomita
Human Metabolome Technologies, Inc., Tsuruoka, Yamagata, Japan
e-mail: ohashi@humanmetabolome.com

Y. Ishihama
Graduate School of Pharmaceutical Sciences, Kyoto University, Kyoto, Japan

H. Onozuka · A. Ochiai · H. Esumi (✉)
National Cancer Center Hospital East, Kashiwa, Chiba, Japan
e-mail: hesumi@ncc.go.jp

1 Introduction

Hyperactivity of glycolysis independent of oxygen availability is a hallmark of cancer metabolism (Warburg effect) (Warburg 1956). Glycolytic energy metabolism of tumor cells is advantageous for perpetual proliferation and meeting the high demand for non-essential amino acids, fatty acids, and nucleotides, although not for efficient production of ATP. Besides glucose, glutamine is significantly consumed by most tumor cells and metabolized to

alanine, lactate, and ammonium ions, which are secreted out of the cells, in a process called glutaminolysis (Heiden et al. 2009). Corroborating these features of cancer metabolism, our previous metabolome analyses of colon and stomach tumor tissues, using capillary electrophoresis time-of-flight mass spectrometry (CE-TOFMS), have revealed significantly high tumor concentrations of glycolytic intermediates including lactate, tricarboxylic acid (TCA) cycle intermediates, and amino acids (Hirayama et al. 2009). Moreover, inter-organ metabolomic differences were more significant than normal-versus-tumor differences within the same organ, which revealed the complexity in generalizing a tumor-specific, organ-independent metabolic profile. This suggested that cells alter their metabolism along with tumorigenesis while retaining much of the metabolism that is unique to their organs of origin. To test this hypothesis further and gain an insight into cancer metabolism, we analyzed metabolomic profiles of normal and tumor tissues obtained from lung and prostate cancer patients.

Deciphering the difference in the flow of energy metabolism between cancer and normal cells solely from the tissue metabolome data is often difficult. The activities of most glycolytic enzymes are known to be regulated by phosphorylation; therefore, we used nano-liquid chromatography-tandem mass spectrometry (nanoLC–MS/MS) to quantify phosphorylation levels of 13 sites contained in ten selected enzymes involved in glycolysis and the TCA cycle. The results indicate that tumor metabolomic profile is highly dependent on its organ of origin, and exhibits unique patterns dependent on cancer type as well as differentiation status. This demonstrates the potential of CE-TOFMS-based metabolomics complemented by phosphorylated enzyme analysis for gaining further insight into the complexity and heterogeneity of tumor metabolism.

2 Materials and methods

2.1 Sampling and metabolite extraction

All the experiments were conducted according to the study protocol that was approved by the Institution Review Board of the National Cancer Center, Japan. Informed consent was obtained from all the participants.

Tumor and surrounding tissues were surgically resected from nine lung and seven prostate cancer patients, who had been administered with no anticancer drugs or medications that could greatly modify their metabolisms previous to the surgical treatments. Clinical information on the patients is listed in Table 1. The resected tissue samples were immediately frozen in liquid nitrogen and stored at −80 °C until metabolite extraction. Sample tissues were weighed and completely homogenized by multi-beads shocker (Yasuikikai, Osaka, Japan) at 2,000 rpm for 3 min, after adding 0.5 ml ice-cold methanol containing 50 μM methionine sulfone and camphor-10-sulfonic acid as internal standards. The homogenates were mixed with 0.5 ml chloroform and 0.2 ml ice-cold Milli-Q water. After centrifugation at 2,300×g for 5 min, the supernatant was centrifugally filtrated through 5-kDa cut-off filters (Millipore, Bedford, MA, USA) at 9,100×g for 3 h to remove proteins. The filtrate was centrifugally concentrated in a vacuum evaporator, dissolved with Milli-Q water, and analyzed by CE-TOFMS.

Table 1 Clinicopathological information of patients and their tumor tissues. W, M, and P in the differentiation status indicate well-, moderately-, and poorly- differentiated tumors, respectively

Organ	ID	Age	Sex	Type	Stage	Differentiation
Lung	L1	82	Male	Squamous cell carcinoma	2B	M
	L2	82	Male	Squamous cell carcinoma	1B	M
	L3	77	Male	Squamous cell carcinoma	1B	P
	L4	80	Female	Adenocarcinoma	1B	M
	L5	78	Male	Pleomorphic carcinoma	3B	N/A
	L6	81	Male	Adenocarcinoma	1A	W
	L7	56	Male	Squamous cell carcinoma	3B	M–P
	L8	61	Male	Large cell carcinoma	1B	N/A
	L9	57	Male	Adenocarcinoma	1B	P
Prostrate	P1	68	Male	Adenocarcinoma	2	M
	P2	66	Male	Adenocarcinoma	2	P
	P3	67	Male	Adenocarcinoma	2	P
	P4	63	Male	Adenocarcinoma	3	P
	P5	62	Male	Adenocarcinoma	2	M
	P6	65	Male	Adenocarcinoma	2	M
	P7	58	Male	Adenocarcinoma	2	M

2.2 CE-TOFMS analysis and data processing

CE-TOFMS analysis was performed by an Agilent CE system combined with a TOFMS (Agilent Technologies, Palo Alto, CA, USA) as described previously (Ohashi et al. 2008) with slight modifications. Cationic metabolites were separated through a fused silica capillary (50 μm internal diameter × 80 cm total length) preconditioned with a commercial buffer (H3301-1001, Human Metabolome Technologies Inc. (HMT), Tsuruoka, Japan) and filled with 1 M formic acid as electrolyte, and a commercial sheath liquid (H3301-1020, HMT) was delivered at a rate of 10 μl/min. Sample solution was injected at a pressure of 50 mbar for 10 s. The applied voltage was set at 30 kV. Electrospray ionization-mass spectrometry (ESI-MS) was conducted in the positive-ion mode and the capillary and fragmentor voltages were set at 4,000 and 120 V, respectively. Nebulizer pressure was configured at 5 psig and N_2 was delivered as a drying gas at a rate of 7 l/min at 300 °C. Exact mass data were acquired at the rate of 1.5 cycles/s over a 50–1,000 *m/z* range. Anionic metabolites were analyzed also through the fused silica capillary preconditioned with a commercial buffer (H3302-1022, HMT) and filled with 50 mM ammonium acetate solution (pH 8.5) as electrolyte, and the aforementioned sheath liquid was delivered at a rate of 10 μl/min. Sample solution was injected at a pressure of 50 mbar for 6 s. The nebulizer pressure, drying gas and its flow rate, applied voltage, and scanning condition of the spectrometer were configured in the same manner as the cationic metabolite analysis. ESI-MS was conducted in the negative mode, and the capillary and fragmentor voltages were set at 3,500 and 125 V, respectively. The data obtained by CE-TOFMS analysis were preprocessed using our proprietary automatic integration software, MasterHands. Each metabolite was identified and quantified based on the peak information including *m/z*, migration time, and peak area. The quantified data were then evaluated for statistical significance by Wilcoxon signed-rank test.

2.3 Enrichment of phosphopeptides

Sample tissues were disrupted by multi-beads shocker and suspended in 100 mM Tris–HCl (pH 9.0) containing 8 M urea, protein phosphatase inhibitors and protein phosphatase inhibitors cocktails (Sigma, St. Louis, MO, USA). After centrifugation at 1,500×*g* for 10 min, the supernatant was reduced with 1 mM dithiothreitol, alkylated with 5 mM iodoacetamide, and then digested with Lys-C endopeptidase at 37 °C for 3 h, followed by 5-fold dilution with 50 mM ammonium bicarbonate and digestion with trypsin at 37 °C overnight. The digested samples were desalted using StageTips with SDB-XC Empore disk membranes (3 M, St. Paul, MN, USA) (Rappsilber et al. 2003).

Phosphopeptides were enriched with hydroxy acid-modified metal oxide chromatography (HAMMOC) (Kyono et al. 2008; Sugiyama et al. 2007). Briefly, custom-made metal oxide chromatography tips were prepared using C8-StageTips and titania beads as described previously (Rappsilber et al. 2007). Prior to loading samples, the tips were equilibrated with 0.1 % trifluoroacetic acid (TFA), 80 % acetonitrile and 300 mg/ml lactic acid (solution A). The digested samples from normal or tumor tissues were diluted with 100 μl solution A and loaded into the HAMMOC tips. After successive washing with solution A and solution B (0.1 % TFA and 80 % acetonitrile), 0.5 % piperidine was used for elution. The eluted fraction was acidified with TFA, desalted using SDB-XC-StageTips, and concentrated in a vacuum evaporator, followed by the addition of solution A for subsequent nanoLC–MS/MS analysis. The phosphopeptide enrichment and sample pretreatment was conducted in duplicate.

2.4 NanoLC–MS/MS analysis and database search

NanoLC–MS/MS analyses were conducted using LTQ-Orbitrap (Thermo Fisher Scientific, Rockwell, IL, USA), a Dionex Ultimate 3000 pump (Thermo Fisher Scientific) and an HTC-PAL autosampler (CTC Analytics, Zwingen, Switzerland). A self-pulled needle (150 mm length × 100 μm internal diameter, 6-μm opening) packed with ReproSil C18 materials (3 μm, Dr. Maisch, Ammerbuch, Germany) was used as an analytical column with "stone-arch" frit (Ishihama et al. 2002). A polytetrafluoroethylene-coated column holder (Nikkyo Technos, Tokyo, Japan) was mounted on an *x–y–z* nanospray interface, and a tee connector with a magnet was used to hold the column needle and to set the appropriate spray position. The injection volume was 5 μl and the flow rate was 500 nl/min for the gradient separation of peptides (Ishihama 2005). The mobile phases consisted of (A) 0.5 % acetic acid and (B) 0.5 % acetic acid and 80 % acetonitrile. A three-step linear gradient of 5–10 % B in 5 min, 10–40 % B in 60 min, 40–100 % B in 5 min and 100 % B in 10 min was used. A spray voltage of 2,400 V was applied via the tee connector. The MS scan range was *m/z* 300–1,500 and the top ten precursor ions were selected for subsequent MS/MS scans. Resolution setting and its maximum injection time were configured at 60,000 and 500 ms, respectively. We also configured the normalized collision energy at 35.0, the isolation width at two, and the minimum signal at 500. Automatic gain controls were set at 500,000 in the MS analysis and at 10,000 in the MS/MS analysis. The capillary temperature was set at 200 °C. A lock mass function was used with a peak derived from polydimethylsiloxane

as a lock mass for the LTQ-Orbitrap to obtain constant mass accuracy during gradient analysis (Olsen et al. 2005). Mass Navigator version 1.2 (Mitsui Knowledge Industry, Tokyo, Japan) was used to create peak lists on the basis of the recorded fragmentation spectra. Peptides and proteins were identified by means of automated database searching using Mascot (Matrix Science, London, UK) against UniProt/Swiss-Prot.

3 Results and discussion

3.1 Overall metabolomic profile and amino acids

We analyzed metabolomic profiles of normal and tumor tissues obtained from nine lung and seven prostate cancer patients by using CE-TOFMS. Based on their *m/z* values and migration times, 114 and 86 metabolites were measured in the lung and prostate tissues, respectively (Supplementary Table S1), and visualized on a metabolome-wide pathway map (Supplementary Fig. S1) using VANTED software (Junker et al. 2006). The metabolomic data were then normalized and hierarchically clustered on both the metabolite and sample axes for a heat map representation (Supplementary Fig. S2) and further analyzed by principal component analysis (PCA) using MeV software (Saeed et al. 2003). Thirty-nine metabolites including glycolytic and TCA cycle intermediates, amino acids, and purine nucleoside phosphates, were absolutely quantified (Supplementary Table S2). PCA indicated that tumor metabolomic profiles were much more heterogeneous than their normal counterparts and comprised multiple clusters (Fig. 1a). With reference to the patient information (Table 1) and the hierarchically-clustered samples (Supplementary Fig. S2), tumor types appeared to play a greater part than tumor stage or differentiation status in altering the overall metabolomic profile in lung cancer, whereas differentiation status contributed more in prostate cancer. Indeed, the cluster of squamous cell carcinoma (SCC) patients (L1–3 and L7) was well-distinguished from that of adenocarcinoma (L4, L6 and L9) and pleomorphic carcinoma (L5). This may reflect the intrinsic pathological difference that adenocarcinoma cells but not squamous carcinoma cells retain their function of secreting mucus as glandular epithelial cells. In prostate samples, poorly differentiated prostate tumors (P2–4) were distant from the cluster of moderately differentiated (P1 and P5–7) tumors, which overlapped with that of normal samples. This may be due to higher duct-forming capacity and hormone response of well-differentiated prostate tumors, as well as normal prostate cells, than that of poorly differentiated tumors.

Both lung and prostate tumor samples were well-separated primarily along the PC1 axis; thus, factor loadings for the PC1 axis were evaluated. Correlations with the PC1 were particularly high in branched-chain amino acids (BCAAs) such as Val ($R = -0.97$), Ile (−0.97), and Leu (−0.89) in lung, and Leu (−0.87) in prostate samples (Supplementary Fig. S3). BCAAs are known to be avidly taken up by tumors and highly oxidized in cancer patients (Baracos and Mackenzie 2006), and thus may serve as effective indicators for diagnosing lung tumors. In fact, average lung tumor concentrations of all the 19 amino acids measured were higher than their respective normal levels, as were average prostate tumor levels of all the amino acids except Asp, Ile and Met (Fig. 1b). This is possibly due to hyperactivity of protein degradation and amino acid transporters in tumor cells (Fuchs and Bode 2005; Vander Heiden et al. 2009). Although average tumor levels of most amino acids in lung samples were significantly higher than their respective normal levels, normal and tumor Asp levels were comparable. Asp may be actively consumed as a precursor for nucleic acids and these TCA cycle intermediates, because tumor concentrations of malate, fumarate and succinate were significantly higher than the normal levels. In prostate tissues, levels of some amino acids such as Asn, Lys, Phe, Ser and Tyr and total essential amino acids were particularly higher in poorly differentiated tumors (P2–4; black in Fig. 1b) than moderately differentiated tumors (P1 and P5–7; gray in Fig. 1b), of which levels were comparable to the corresponding normal levels (Fig. 1b), implying enhancement of acquiring the amino acids upon dedifferentiation of prostate cancer cells.

3.2 Energy charge and adenosine and guanosine phosphates

Adenylate and guanylate energy charges (([RTP] + 0.5 × [RDP])/([RTP] + [RDP] + [RMP]), R = A or G) were lower in lung tumor than normal tissues (Fig. 2a); however, tumor levels were significantly higher than normal levels for ATP (3.8-fold), GTP (4.2-fold), and the other adenosine and guanosine phosphates (1.9–7.9-fold), and hence total adenylates (4.5-fold) and guanylates (4.0-fold). Tumor concentrations of these metabolites were relatively higher in all the SCC samples (L1–3 and L7; black in Fig. 2a) than the others (gray in Fig. 2a) such as L5 and L6, whose overall tumor metabolomic profiles resembled their respective normal profiles (Fig. 1). Purine synthesis may thus be hyperactivated in lung tumors, especially SCC, probably with a high basal ATP ↔ ADP turnover and purine salvage for maximizing their growth. Although prostate tissues showed much less normal-versus-tumor

differences, tumor ADP level was significantly lower than normal level (Fig. 2b). High absolute concentrations of ADP and GDP among other purine nucleoside phosphates are unique to prostate tissues, and ATP and AMP levels were relatively higher in poorly differentiated tumors (P2–4; black in Fig. 2b) than moderately differentiated tumors (P1 and P5–7; gray in Fig. 2b). This might be due to a differential expression of adenylate kinase catalyzing the reaction, 2ADP ↔ ATP + AMP, which is undetectable in adult prostate but shows activity along with its malignant alteration (Hall et al. 1985).

3.3 Glycolytic and TCA cycle intermediates and phosphorylated enzymes

Most glycolytic and TCA cycle intermediates were absolutely quantified (Fig. 3a), and phosphorylation levels of associated enzymes were also examined (Fig. 3b). Tumor lactate levels were higher than normal levels in both lung and prostate tissues, indicating their enhanced glycolysis and lactate fermentation, which reaffirmed the Warburg effect in cancer. Lung tumor levels of fructose 6-phosphate and fructose 1,6-bisphosphate were significantly lower and higher, respectively, than their corresponding normal levels. This may be partly explained by significantly high tumor levels of S386 phosphorylation in phosphofructokinase, which enhances its activity (Brand and Soling 1975), and thus the overall glycolytic flux because it is a bottleneck enzyme. Although tumor levels of S83 phosphorylation in glyceraldehyde 3-phosphate dehydrogenase and S203 in phosphoglycerate kinase-1 were significantly higher than their respective normal levels, their functional impacts are unknown. Tumor level of S37 phosphorylation of pyruvate kinase, which enhances its activity (Le Mellay et al. 2002), was significantly higher than the normal level. This may rationalize the trend that phosphoenolpyruvate and pyruvate were significantly lower and higher, respectively, in tumor than normal tissues. Tumor levels of S293 and S291 phosphorylation in pyruvate dehydrogenase, which inhibit its activity (Korotchkina and Patel 2001; Patel and Korotchkina 2001), were significantly higher than normal levels in all the lung cancer patients, except L6. This inhibition may contribute to the enhanced glycolysis and resulting lactate accumulation in lung tumors. In prostate tissues, however, most glycolytic intermediates were not detected, probably owing to inevitable overdilution of the samples for reducing polyamine concentrations, which otherwise adversely interfere with CE-TOFMS analysis. Trivial differences were observed between normal and tumor prostate phosphorylation levels of most glycolytic enzymes except glucose 6-phosphate isomerase (G6PI); nevertheless, the impact of elevated phosphorylation on the activity of G6PI is uncertain. Although intriguing, there was no apparent correlation between significantly high tumor levels of S481 phosphorylation in ATP citrate lyase in SCC samples, L1, L3

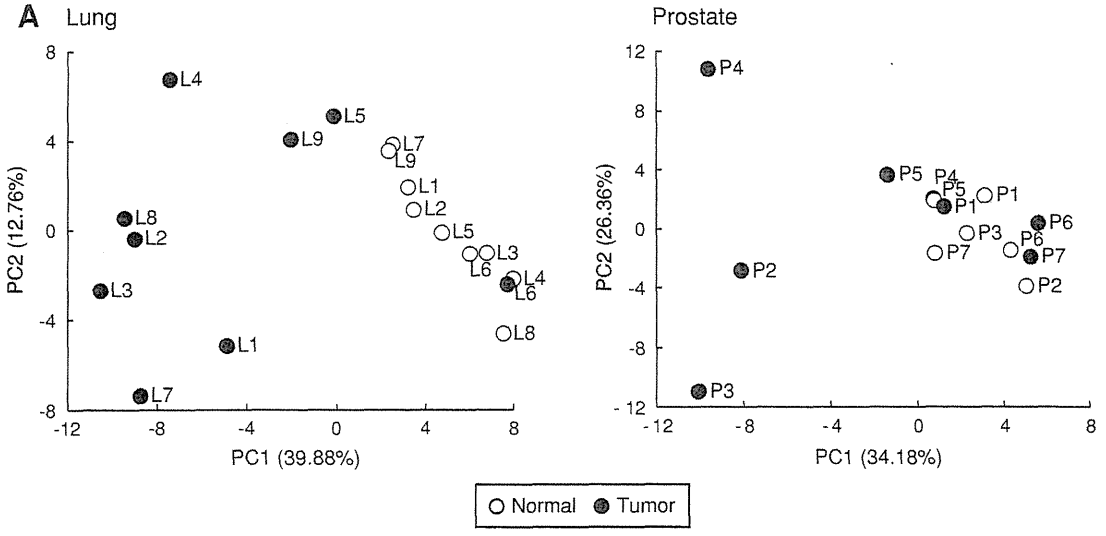

Fig. 1 **a** Score plots of PCA using the normalized metabolomic data of paired normal and tumor tissues obtained from lung (*left*) and prostate (*right*) cancer patients. The sample codes correspond to the patient IDs listed in Table 1. *Percentage values* indicated on the axes represent the contribution rate of the first (PC1) and the second (PC2) principal components. **b** Quantified levels of amino acids in normal (*left, open dots*) and tumor (*right, filled dots*) tissues obtained from lung and prostate cancer patients. *Horizontal bars* represent mean ± SD of normal (*left*) and tumor (*right*) samples and each connected pair represents the values for the same patient. *Gray dots* represent the values for patients with non-SCC lung cancer (L4–L6, L8 and L9) and patients with moderately differentiated prostate cancer (P1 and P5–7). *N.D.* indicates that the metabolite level was below the detection limit of the analysis. *Asterisks* indicate the significant differences between normal and tumor tissue levels based on the Wilcoxon signed-rank test (*$p < 0.05$; **$p < 0.01$; and ***$p < 0.001$)

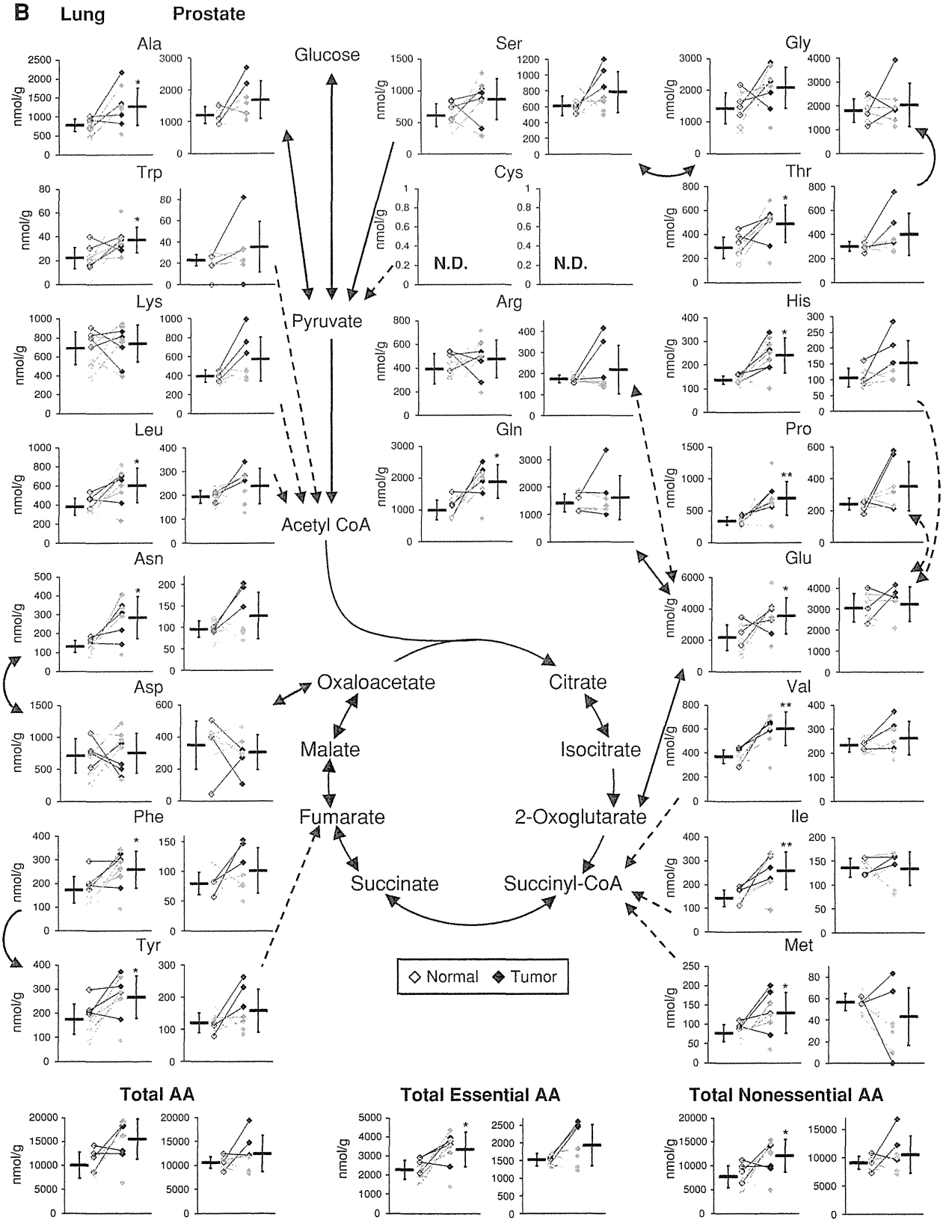

Fig. 1 continued

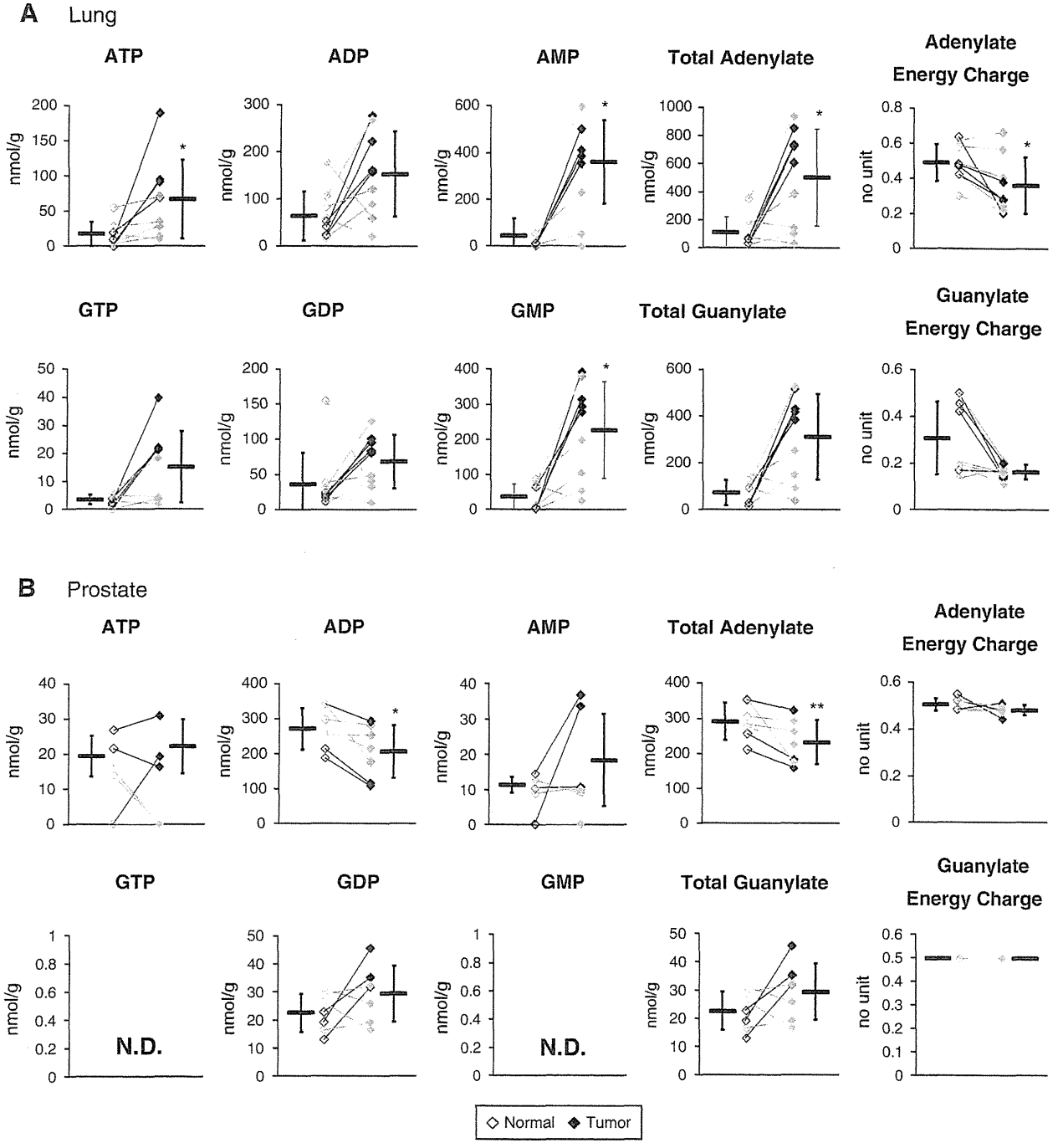

Fig. 2 Adenosine and guanosine phosphates, total adenylates and guanylates, and adenylate and guanylate energy charges of normal (*left, open dots*) and tumor (*right, filled dots*) tissues obtained from lung (**a**) and prostate (**b**) cancer patients. *Horizontal bars* represent mean ± SD of normal (*left*) and tumor (*right*) samples and each connected pair represents the values for the same patient. *Gray dots* represent the values for patients with non-SCC lung cancer (L4–L6, L8 and L9) and patients with moderately differentiated prostate cancer (P1 and P5–7). *N.D.* indicates that the metabolite level was below the detection limit of the analysis. *Asterisks* indicate the significant differences between normal and tumor tissue levels based on the Wilcoxon signed-rank test ($*p < 0.05$; $**p < 0.01$; and $***p < 0.001$)

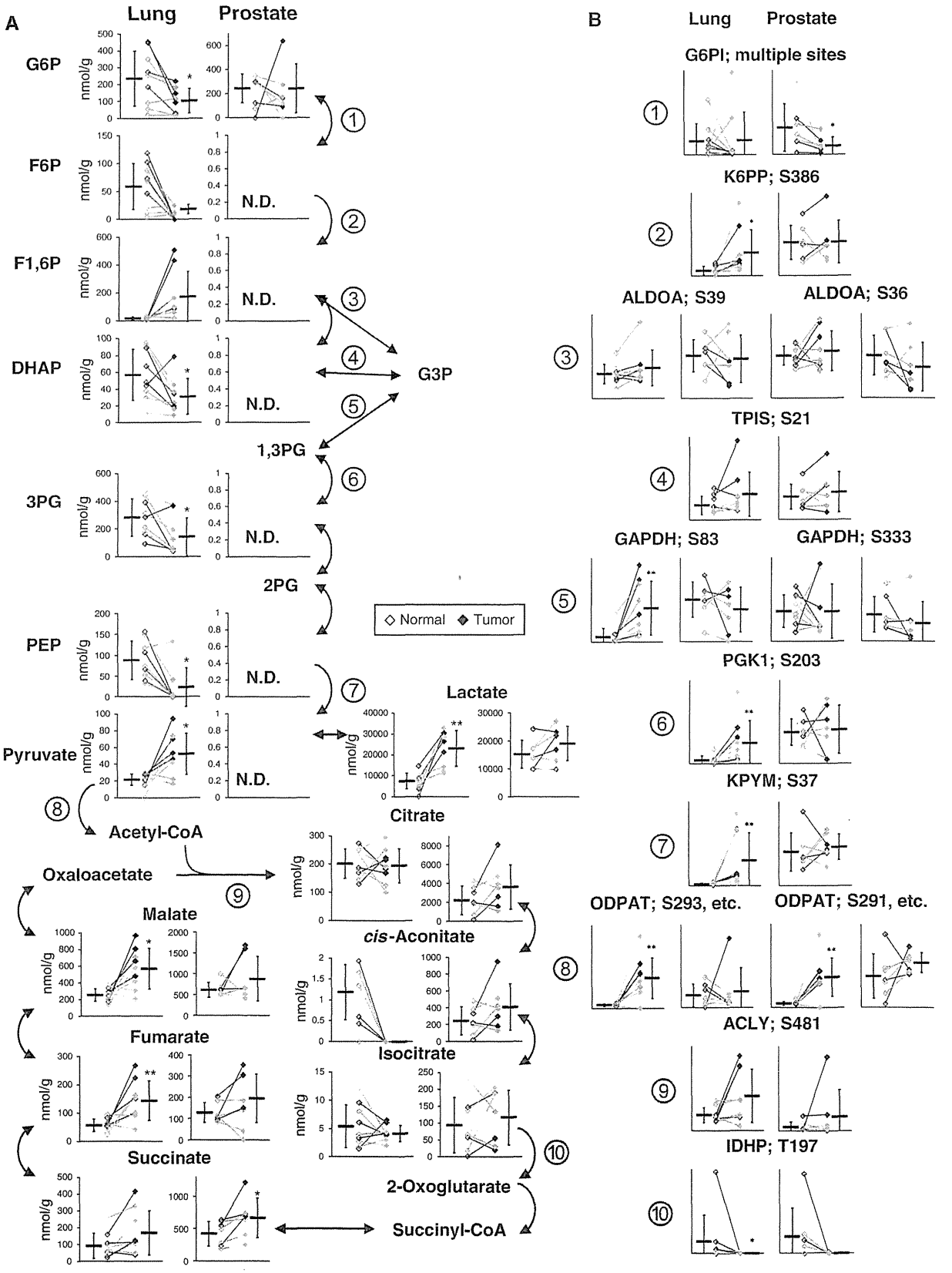
A
Lung
Prostate
G6P
F6P
F1,6P
DHAP
G3P
1,3PG
3PG
2PG
PEP
Pyruvate
Lactate
Citrate
Acetyl-CoA
Oxaloacetate
Malate
Fumarate
Succinate
cis-Aconitate
Isocitrate
2-Oxoglutarate
Succinyl-CoA
N.D.
nmol/g
◇ Normal ◆ Tumor
B
Lung
Prostate
G6PI; multiple sites
K6PP; S386
ALDOA; S39
ALDOA; S36
TPIS; S21
GAPDH; S83
GAPDH; S333
PGK1; S203
KPYM; S37
ODPAT; S293, etc.
ODPAT; S291, etc.
ACLY; S481
IDHP; T197

◀ **Fig. 3** Quantified levels of glycolytic and TCA cycle intermediates (**a**) and phosphorylation levels of each phosphorylation site in associated enzymes (**b**) in normal (*left, open dots*) and tumor (*right, filled dots*) tissues obtained from lung and prostate cancer patients. *Encircled numbers* in (**a**) indicated next to the metabolic reactions involved in glycolysis and the TCA cycle correspond to the associated enzymes in (**b**). *Horizontal bars* represent mean ± SD of normal (*left*) and tumor (*right*) samples and each connected pair represents the values for the same patient. *Gray dots* represent the values for patients with non-SCC lung cancer (L4–L6, L8 and L9) and patients with moderately differentiated prostate cancer (P1 and P5–7). *N.D.* indicates that the metabolite level was below the detection limit of the analysis. *Asterisks* indicate the significant differences between normal and tumor tissue levels based on the Wilcoxon signed-rank test (*$p < 0.05$; **$p < 0.01$; and ***$p < 0.001$). *G6PI* glucose 6-phosphate isomerase; *K6PP* 6-phosphofructokinase; *ALDOA* aldolase A; *TPIS* triosephosphate isomerase; *GAPDH* glyceraldehydes 3-phosphate dehydrogenase; *PGK1* phosphoglycerate kinase 1; *KPYM* pyruvate kinase isozymes M1/M2; *ODPAT* pyruvate dehydrogenase E1 component subunit alpha; *ACLY* ATP-citrate synthase; and *IDHP* isocitrate dehydrogenase

and L7, and their citrate concentrations. The impact of elevated phosphorylation levels of T197 in isocitrate dehydrogenase in normal L2 and P2 samples was also unclear. We need a larger number of sample sets in order to validate these results and provide further insight into possible correlations between phosphorylated states of the enzymes and metabolomic profiles.

Levels of all the quantified TCA cycle intermediates were higher in tumor than normal prostate tissues (Fig. 3a), which may be related to the typically hypoxic microenvironment of prostate tissues, because most TCA cycle intermediates are known to increase under hypoxia, while their flux through the pathway remains low (Wiebe et al. 2008). Average prostate citrate concentrations were >11-fold higher than in lung. This was partly due to a high concentration of zinc in the prostate, which inhibits m-aconitase and results in citrate accumulation (Mycielska et al. 2009). Prostate tumor exhibits low zinc levels and elevated fatty acid synthesis consuming citrate, and thus its citrate level is typically lower than in normal tissues (Mycielska et al. 2009), which is, however, inconsistent with our results. Tumor citrate, *cis*-aconitate, and isocitrate levels in P1, P3 and P7 were consistently lower than their respective normal levels, leaving the possibility that zinc and m-aconitase activity levels may vary depending on a factor other than differentiation status.

Succinate, fumarate, and malate levels were markedly higher in both prostate and lung tumor tissues than their corresponding normal tissues (Fig. 3a), which was consistent with our previous results for colon and stomach tumor metabolomics (Hirayama et al. 2009). We recently obtained strong evidence that, especially under hypoxic and nutrient-deprived conditions, energy generation of cancer relies on fumarate respiration (Sakai et al. 2012; Tomitsuka et al. 2010). This confers upon cells the ability to produce ATP by harnessing fumarate to succinate conversion, rather than oxygen to water, as the final electron transport step via the reverse reaction of succinate dehydrogenase (Kita and Takamiya 2002). Accumulation of these metabolites in tumors may therefore be attributed to hyperactivity of fumarate respiration.

3.4 Tumor-specificity and organ-dependency in metabolic profiles

The metabolome data obtained from both lung and prostate tissues were collectively normalized and hierarchically clustered (Supplementary Fig. S4A). As a result, lung-versus-prostate differences in terms of the overall metabolomic profiles appeared to be more significant than normal-versus-tumor differences within the same organ, as observed in our previous comparative metabolome analyses in colon and stomach tissues (Hirayama et al. 2009). As expected, PCA with the collectively normalized data showed clear inter-organ differences along with the PC2 axis; however, the normal-versus-tumor distinctions were also observed along with the PC1 axis (Supplementary Fig. S4B). This suggests that, in the carcinogenic process, cells alter their metabolism with a certain 'metabolic directionality' that is independent of organ types while retaining much of the metabolism that is unique to their organs of origin. Metabolites that showed high correlations with the PC2 included several nucleosides, TCA cycle intermediates, and polyamines, which characterize the inter-organ metabolic differences (Supplementary Table S3). In contrast, most glucogenic amino acids such as Thr, Ile, Asn, Pro, His, Gln, and Ser were closely associated with the PC1 (Supplementary Table S3), suggesting that a hyper-production and/or -acquisition of a certain set of amino acids likely occurs in the course of tumorigenesis.

4 Conclusion

Overall tumor metabolomic profiles were found to be significantly different depending on tumor type in lung cancer and differentiation status in prostate cancer. Elevated tumor concentrations of almost all the amino acids, especially BCAAs, were identified in an organ-independent manner, and this trend was more prominent in SCC than the other tumor types in lung cancer and in poorly rather than moderately differentiated prostate cancer. Analyses with much more samples, however, are necessary in order to statistically confirm these unique subtype-specific metabolic fingerprint of cancer. In contrast, through our combined metabolomic and phosphorylated enzyme analyses, we found that glycolytic and TCA cycle intermediates,

levels of which are probably associated with enzyme phosphorylation levels, exhibited significant organ dependency, reaffirming that inter-organ metabolomic differences are generally more significant than normal-versus-tumor differences within the same organ. Nonetheless, metabolomic profiles of both lung and prostate tumors appear to have a common 'directionality' along with their increasing malignancy represented by high concentrations of a certain set of glucogenic amino acids. Taken together, we identified organ-dependent, tumor-specific, and tumor-pathology-dependent metabolic features, which highlights the need for a combined metabolomics and phosphoproteomics analysis on a broader scale with a larger number of sample sets for improving specificity and effectiveness of personalized anticancer therapeutics.

Acknowledgments The authors thank Dr. Masahiro Sugimoto for developing MasterHands software. This work was supported in part by a grant for the Third Term Comprehensive 10-year Strategy for Cancer Control from the Ministry of Health, Labour and Welfare (H.E.) and a grant from the Global COE Program entitled, "Human Metabolomic Systems Biology" (K.K.). This work was also supported by KAKENHI (Grant-in-Aid for Scientific Research) on Priority Areas "Systems Genomes" and on "Lifesurveyor" from the Ministry of Education, Culture, Sports, Science and Technology (MEXT) of Japan as well as research funds from the Yamagata prefectural government and the City of Tsuruoka (Y.O., M.T., and T.S.).

References

Baracos, V. E., & Mackenzie, M. L. (2006). Investigations of branched-chain amino acids and their metabolites in animal models of cancer. *Journal of Nutrition, 136*, 237S–242S.

Brand, I. A., & Soling, H. D. (1975). Activation and inactivation of rat liver phosphofructokinase by phosphorylation--dephosphorylation. *FEBS Letters, 57*, 163–168.

Fuchs, B. C., & Bode, B. P. (2005). Amino acid transporters ASCT2 and LAT1 in cancer: Partners in crime? *Seminars in Cancer Biology, 15*, 254–266.

Hall, M., Mickey, D. D., Wenger, A. S., & Silverman, L. M. (1985). Adenylate kinase: An oncodevelopmental marker in an animal model for human prostatic cancer. *Clinical Chemistry, 31*, 1689–1691.

Heiden, M. G. V., Cantley, L. C., & Thompson, C. B. (2009). Understanding the Warburg effect: The metabolic requirements of cell proliferation. *Science, 324*, 1029–1033.

Hirayama, A., Kami, K., Sugimoto, M., Sugawara, M., Toki, N., Onozuka, H., et al. (2009). Quantitative metabolome profiling of colon and stomach cancer microenvironment by capillary electrophoresis time-of-flight mass spectrometry. *Cancer Research, 69*, 4918–4925.

Ishihama, Y. (2005). Proteomic LC-MS systems using nanoscale liquid chromatography with tandem mass spectrometry. *Journal of Chromatography A, 1067*, 73–83.

Ishihama, Y., Rappsilber, J., Andersen, J. S., & Mann, M. (2002). Microcolumns with self-assembled particle frits for proteomics. *Journal of Chromatography A, 979*, 233–239.

Junker, B. H., Klukas, C., & Schreiber, F. (2006). VANTED: A system for advanced data analysis and visualization in the context of biological networks. *BMC Bioinformatics, 7*, 109.

Kita, K., & Takamiya, S. (2002). Electron-transfer complexes in *Ascaris* mitochondria. *Advances in Parasitology, 51*, 95–131.

Korotchkina, L. G., & Patel, M. S. (2001). Site specificity of four pyruvate dehydrogenase kinase isoenzymes toward the three phosphorylation sites of human pyruvate dehydrogenase. *Journal of Biological Chemistry, 276*, 37223–37229.

Kyono, Y., Sugiyama, N., Imami, K., Tomita, M., & Ishihama, Y. (2008). Successive and selective release of phosphorylated peptides captured by hydroxy acid-modified metal oxide chromatography. *Journal of Proteome Research, 7*, 4585–4593.

Le Mellay, V., Houben, R., Troppmair, J., Hagemann, C., Mazurek, S., Frey, U., et al. (2002). Regulation of glycolysis by Raf protein serine/threonine kinases. *Advances in Enzyme Regulation, 42*, 317–332.

Mycielska, M. E., Patel, A., Rizaner, N., Mazurek, M. P., Keun, H., Ganapathy, V., et al. (2009). Citrate transport and metabolism in mammalian cells: Prostate epithelial cells and prostate cancer. *BioEssays, 31*, 10–20.

Ohashi, Y., Hirayama, A., Ishikawa, T., Nakamura, S., Shimizu, K., Ueno, Y., et al. (2008). Depiction of metabolome changes in histidine-starved *Escherichia coli* by CE-TOFMS. *Molecular BioSystems, 4*, 135–147.

Olsen, J. V., de Godoy, L. M., Li, G., Macek, B., Mortensen, P., Pesch, R., et al. (2005). Parts per million mass accuracy on an Orbitrap mass spectrometer via lock mass injection into a C-trap. *Molecular and Cellular Proteomics, 4*, 2010–2021.

Patel, M. S., & Korotchkina, L. G. (2001). Regulation of mammalian pyruvate dehydrogenase complex by phosphorylation: Complexity of multiple phosphorylation sites and kinases. *Experimental & Molecular Medicine, 33*, 191–197.

Rappsilber, J., Ishihama, Y., & Mann, M. (2003). Stop and go extraction tips for matrix-assisted laser desorption/ionization, nanoelectrospray, and LC/MS sample pretreatment in proteomics. *Analytical Chemistry, 75*, 663–670.

Rappsilber, J., Mann, M., & Ishihama, Y. (2007). Protocol for micro-purification, enrichment, pre-fractionation and storage of peptides for proteomics using StageTips. *Nature Protocols, 2*, 1896–1906.

Saeed, A. I., Sharov, V., White, J., Li, J., Liang, W., Bhagabati, N., et al. (2003). TM4: A free, open-source system for microarray data management and analysis. *BioTechniques, 34*, 374–378.

Sakai, C., Tomitsuka, E., Esumi, H., Harada, S., & Kita, K. (2012). Mitochondrial fumarate reductase as a target of chemotherapy: From parasites to cancer cells. *Biochimica et Biophysica Acta, 1820*, 643–651.

Sugiyama, N., Masuda, T., Shinoda, K., Nakamura, A., Tomita, M., & Ishihama, Y. (2007). Phosphopeptide enrichment by aliphatic hydroxy acid-modified metal oxide chromatography for nano-LC-MS/MS in proteomics applications. *Molecular and Cellular Proteomics, 6*, 1103–1109.

Tomitsuka, E., Kita, K., & Esumi, H. (2010). The NADH-fumarate reductase system, a novel mitochondrial energy metabolism, is a new target for anticancer therapy in tumor microenvironments. *Annals of the New York Academy of Sciences, 1201*, 44–49.

Warburg, O. (1956). On the origin of cancer cells. *Science, 123*, 309–314.

Wiebe, M. G., Rintala, E., Tamminen, A., Simolin, H., Salusjarvi, L., Toivari, M., et al. (2008). Central carbon metabolism of *Saccharomyces cerevisiae* in anaerobic, oxygen-limited and fully aerobic steady-state conditions and following a shift to anaerobic conditions. *FEMS Yeast Research, 8*, 140–154.

European Journal of Medicinal Chemistry 60 (2013) 76–88

Contents lists available at SciVerse ScienceDirect

European Journal of Medicinal Chemistry

journal homepage: http://www.elsevier.com/locate/ejmech

Original article

Synthesis and antitumor evaluation of arctigenin derivatives based on antiausterity strategy

Naoki Kudou [a], Akira Taniguchi [b], Kenji Sugimoto [a], Yuji Matsuya [a], Masashi Kawasaki [c], Naoki Toyooka [b,d,*], Chika Miyoshi [e], Suresh Awale [f], Dya Fita Dibwe [g], Hiroyasu Esumi [e], Shigetoshi Kadota [g], Yasuhiro Tezuka [g,**]

[a] Graduate School of Medicine and Pharmaceutical Sciences, University of Toyama, 2630 Sugitani, Toyama, 930-0194, Japan
[b] Graduate School of Science and Technology for Research, University of Toyama, 3190 Gofuku, Toyama 930-8555, Japan
[c] Department of Liberal Arts and Sciences, Faculty of Engineering, Toyama Prefectural University, 5180 Kurokawa, Kosugi-Machi, Toyama 939-0398, Japan
[d] Graduate School of Innovative Life Science, University of Toyama, 3190 Gofuku, Toyama 930-8555, Japan
[e] Cancer Physiology Project, Research Center for Innovative Oncology, National Cancer Center Hospital East, Chiba, Japan
[f] Frontier Research Core for Life Sciences, University of Toyama, 2630 Sugitani, Toyama 930-0194, Japan
[g] Institute of Natural Medicine, University of Toyama, 2630 Sugitani, Toyama 930-0194, Japan

ARTICLE INFO

Article history:
Received 24 July 2012
Received in revised form
14 September 2012
Accepted 21 November 2012
Available online 28 November 2012

Keywords:
(−)-Arctigenin derivatives
Antiausteric activity
Synthesis
Pancreatic cancer

ABSTRACT

A series of new (−)-arctigenin derivatives with variably modified *O*-alkyl groups were synthesized and their preferential cytotoxicity was evaluated against human pancreatic cancer cell line PANC-1 under nutrient-deprived conditions. The results showed that monoethoxy derivative **4i** (PC_{50}, 0.49 μM), diethoxy derivative **4h** (PC_{50}, 0.66 μM), and triethoxy derivative **4m** (PC_{50}, 0.78 μM) showed the preferential cytotoxicities under nutrient-deprived conditions, which were identical to or more potent than (−)-arctigenin (**1**) (PC_{50}, 0.80 μM). Among them, we selected the triethoxy derivative **4m** and examined its *in vivo* antitumor activity using a mouse xenograft model. Triethoxy derivative **4m** exhibited also *in vivo* antitumor activity with the potency identical to or slightly more than (−)-arctigenin (**1**). These results would suggest that a modification of (−)-arctigenin structure could lead to a new drug based on the antiausterity strategy.

1. Introduction

Pancreatic cancer is the most aggressive cancer of all and has an exceptionally high global mortality rate, with an estimated 267,000 deaths worldwide in 2008. It ranks 8th or 9th as the most frequent cause of cancer death worldwide and is the 4th or 5th most frequent cause of cancer death in most developed countries, including the United States, Europe, and Japan [1]. Moreover, it has been estimated that the number of deaths from pancreatic cancer will reach 484,000 by 2030 [1]. Pancreatic cancer rapidly metastases and lead the patients to die in a short period of the diagnosis. Thus, the 5-year survival rate of the patients with the pancreatic cancer is the lowest among several cancers [2,3]. Though surgery is the only treatment method that offers any prospect of potential cure, chemotherapy with 5-fluorouracil and gemcitabine is also used for palliative therapy of advanced pancreatic cancer. However pancreatic cancer is largely resistant to most known chemotherapeutic agents including 5-fluorouracil and gemcitabine [4]. Therefore effective chemotherapeutic agents that target pancreatic cancer are urgently needed.

Tumor cells, in general, proliferate very fast, and the demand for essential nutrients, oxygen, *etc.* is always high. The immediate environment of cancers increasing in size, however, often becomes heterogeneous and some regions of large cancers often possess microenvironmental niches, which exhibit a significant gradient of critical metabolites including oxygen, glucose, other nutrients, and growth factors [5]. Thus, many cancer cells get the critical metabolites by randomly recruiting new blood vessels, a phenomenon commonly known as angiogenesis, to survive under such severe conditions. However, human pancreatic cancer survives with an extremely poor blood supply and becomes more malignant [6]. The method by which pancreatic cancer survives is by getting a remarkable tolerance to extreme nutrient starvation [7]. Therefore, it has been hypothesized that eliminating the tolerance of cancer cells to nutrition starvation

* Corresponding author. Graduate School of Science and Technology for Research, University of Toyama, 3190 Gofuku, Toyama 930-8555, Japan. Tel.: +81 76 445 6859.
** Corresponding author. Tel.: +81 76 434 7627; fax: +81 76 434 5059.
E-mail addresses: toyooka@eng.u-toyama.ac.jp (N. Toyooka), tezuka@inm.u-toyama.ac.jp (Y. Tezuka).

0223-5234/$ – see front matter © 2012 Elsevier Masson SAS. All rights reserved.
http://dx.doi.org/10.1016/j.ejmech.2012.11.031

may allow a novel biochemical approach known as "anti-austerity" for cancer therapy [8].

In this regard, we screened 500 medicinal plants used in Kampo medicine to identify agents that preferentially reduce the survival of nutrient-deprived human pancreatic cancer PANC-1 cells. The screen led to the isolation of (−)-arctigenin (**1**) as the active principle of *Arctium lappa* [9]. In addition to pancreatic cancer, arctigenin has been reported to inhibit lung, skin, and stomach cancers [10]. Thus, we started the synthetic work of arctigenin derivatives to obtain more effective drugs against pancreatic cancer. In *A. lappa*, (−)-arctigenin is mainly contained as its glucoside, arctiin, and after consumption arctiin was reported to be deglucosidated to (−)-arctigenin (**1**), followed by demethylation and dehydroxylation by intestinal bacteria to metabolites **I**–**V** [11]. As reported previously, (−)-arctigenin showed potent preferential cytotoxicity, whereas its glucoside, arctiin, showed no cytotoxicity [9]. In our preliminary examination, moreover, metabolites **I** and **V** (Fig. 1) showed weaker activity. These facts should suggest that the 4′-hydroxyl group should be important for the preferential cytotoxicity and that (−)-arctigenin is deactivated through the demethylation/demethoxylation. In addition, the enantiomer of (−)-arctigenin (**1**), (+)-arctigenin (Fig. 1), showed very weak preferential cytotoxicity, indicating the importance of the 2*R*,3*R* absolute stereochemistry of (−)-form. Thus, with an intention to improve the metabolism stability, we have synthesized 15 arctigenin derivatives **4a**–**o** with different alkoxy substituent and the 2*R*,3*R*-configuration, and the *in vitro* preferential cytotoxicity of them was characterized under nutrient-deprived conditions. Then, the triethoxy derivative **4m**, exhibiting the *in vitro* activity identical to **1** and having no methoxy group which may be metabolized, was selected and further evaluated the effect against tumor cell growth *in vivo* in a cancer xenograft mouse model.

2. Results and discussion

2.1. Chemistry

First we planned the synthesis of derivatives on the 3′ position of (−)-arctigenin. For this purpose, (−)-arctigenin (**1**) was converted to the diol **2** [12], which was transformed into 6 derivatives **4a**–**f** via selective protection of **2**, alkylation of **3**, followed by deprotection of the benzyl group (Scheme 1).

Next we planned the efficient and flexible synthesis of a variety of derivatives on the 3′, 3″, and 4″ positions of (−)-arctigenin.

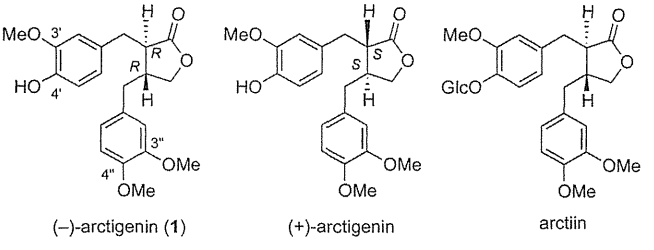

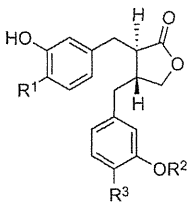

	R^1	R^2	R^3
I	OH	Me	OMe
II	H	Me	OMe
III	H	H	OMe
IV	H	H	OH
V	H	H	H

Fig. 1. Structures of (−)-arctigenin (**1**) and its analogs.

3,4-Dihydroxybenzaldehyde was converted to the alcohol **7** via known benzyl ether **5** [13] and aldehyde **6** [14]. Mono-alkylation of diethyl malonate with the mesylate of **7** afforded the ester **8**. Reduction of **8** and lipase-mediated transesterification of the resulting diol provided the mono-acetate (+)-**9**. The enantiomeric excess of (+)-**9** was determined to be 98% ee by the HPLC analysis using the chiral column (Chiralcel OJ). The absolute stereochemistry of (+)-**9** was determined by the comparison of the optical rotation with known lactone **13a**, prepared from (+)-**9** via mesylate **10**, benzyl ether **11**, and lactone **12a** as shown in Scheme 2. Other lactones **13b**–**f** were also prepared from (+)-**9**, and these lactones **13b**–**f** were alkylated on the α-position with several alkyl halides to afford the di-substituted lactones **14a**–**i**. Finally deprotection of the benzyl group furnished the desired derivatives **4g**–**o**.

From the comparison of the *in vitro* activity of the synthesized derivatives **4a**–**o** against the human pancreatic cancer cell line PANC-1, the triethoxy derivative **4m** was chosen as the potent candidate for the *in vivo* experiment. As the more effective synthesis of **4m**, we investigated the modified synthesis of the lactone **13d**. 3,4-Dihydroxybenzaldehyde was converted to the ester **17** via known aldehyde **15** [15] and alcohol **16** [16] as the same procedure for the synthesis of **8**. After reduction of **17**, lipase-mediated transesterification of the resulting diol afforded the mono-acetate **18**, whose enantiomeric excess was determined to be 98% ee again by the Mosher method. The mono-acetate **18** was then transformed into the lactone **13d** via mesylate **19** (Scheme 3).

2.2. In vitro preferential cytotoxicity of arctigenin derivatives

All of the (−)-arctigenin derivatives **4a**–**o** were evaluated for their *in vitro* preferential cytotoxic activity against human pancreatic cancer PANC-1 cells in nutrient-deprived medium (NDM). The PANC-1 cell line is highly resistant to nutrient starvation, and can survive in NDM even after 48 h of starvation [6,7,8]. However, this tolerance to nutrient starvation was remarkably eliminated by the tested compounds in a concentration-dependent manner. The tested compounds exhibited different potency of toxicity (Fig. 2) and their preferential cytotoxicities are obtained as the 50% cytotoxic concentration in NDM (PC_{50} value) (Table 1). Among the (−)-arctigenin derivatives **4a**–**o**, monoethoxy derivative **4i** showed the most potent preferential cytotoxicity (PC_{50}, 0.49 μM), followed by diethoxy derivative **4h** (PC_{50}, 0.66 μM) and triethoxy derivative **4m** (PC_{50}, 0.78 μM), which were identical to or more potent than (−)-arctigenin (**1**) (PC_{50}, 0.80 μM).

On the relationship between the substituents and the preferential activity, the 3′ position seems to favor smaller substituent since the PC_{50} values of **1** and **4a**–**d** increase in the order: **1** (MeO) < **4a** (EtO) = **4b** (*n*-PrO) < **4c** (*i*-PrO) < **4d** (*n*-BuO). This would suggest the importance of the 4′-hydroxy group for the preferential activity. On the other hand, there is not clear relationship on the substituents at the 3″ and 4″ positions, although smaller substituents seems to be favor.

The order of *in vitro* preferential cytotoxicity (PC_{50}) was **4i** > **4h** > **4m**. Whereas **4h** and **4i** have the methoxy groups which was reported to be demethylated and then deoxygenated by intestinal bacteria and/or hepatic enzyme [11]. Thus, we selected the triethoxy derivative **4m** to pursue a further examination, from a viewpoint of metabolism stability.

2.3. In vivo antitumor activity of triethoxy derivative 4m

The triethoxy derivative **4m** showed the *in vitro* preferential cytotoxicity also against human pancreatic cancer cell line CAPAN-1 under glucose deficient conditions with a intensity similar to (−)-arctigenin (**1**) (Fig. 3). We used PANC-1 cell line for *in vitro*

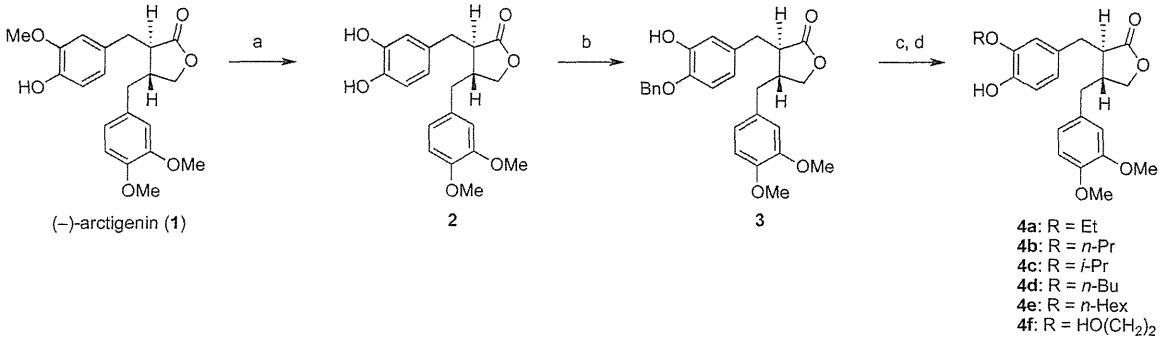

Scheme 1. Reagents and conditions: a: $AlCl_3$, pyridine, CH_2Cl_2, reflux (quant.); b: BnBr, K_2CO_3, KI, acetone, reflux (63%); c: RI or RBr, K_2CO_3, acetone, reflux for **4a–e** or 2-benzyloxyethanol, Ph_3P, DEAD, CH_2Cl_2, rt for **4f**; d: H_2, $Pd(OH)_2$, MeOH, rt.

study because of its ready growth [17], while mouse xenograft model can be prepared with CAPAN-1 cell line more easily than with PANC-1 cell line [18]. Thus, we used mouse xenograft model with CAPAN-1 cell line for comparing the *in vivo* effect of triethoxy derivative **4m** with (−)-arctigenin (**1**).

Mice were inoculated with 5×10^6 CAPAN-1 cells s.c. on the back and then administered triethoxy derivative **4m**, (−)-arctigenin (**1**), or vehicle, as described in Experimental. The body weight of the animals was monitored weekly (Fig. 4A) and no significant body weight loss was recognized in the treated group versus the vehicle control group at any time during the experimental period. This fact, together with the behavior of the treated animals, indicated that the tested compounds might have no toxicity at the dose used. The treatment was initiated from the 15th day by i.p. injection of the drug at the dose of 50 μg/mouse/d on 6 days of the week (or vehicle in the control group) until the 28th day. The tumor size was measured weekly. As is evident from the tumor growth curve shown in Fig. 4B, the tumor volume increased steadily in the control group, whereas the increase was significantly less prominent in the groups treated by triethoxy derivative **4m** or (−)-arctigenin (**1**). There was a significant difference in the tumor size at the day 21 between the groups treated by triethoxy derivative **4m** or (−)-arctigenin (**1**) and the control group ($P < 0.05$). Similarly, the mean wet weight and the size of the tumor were higher in the

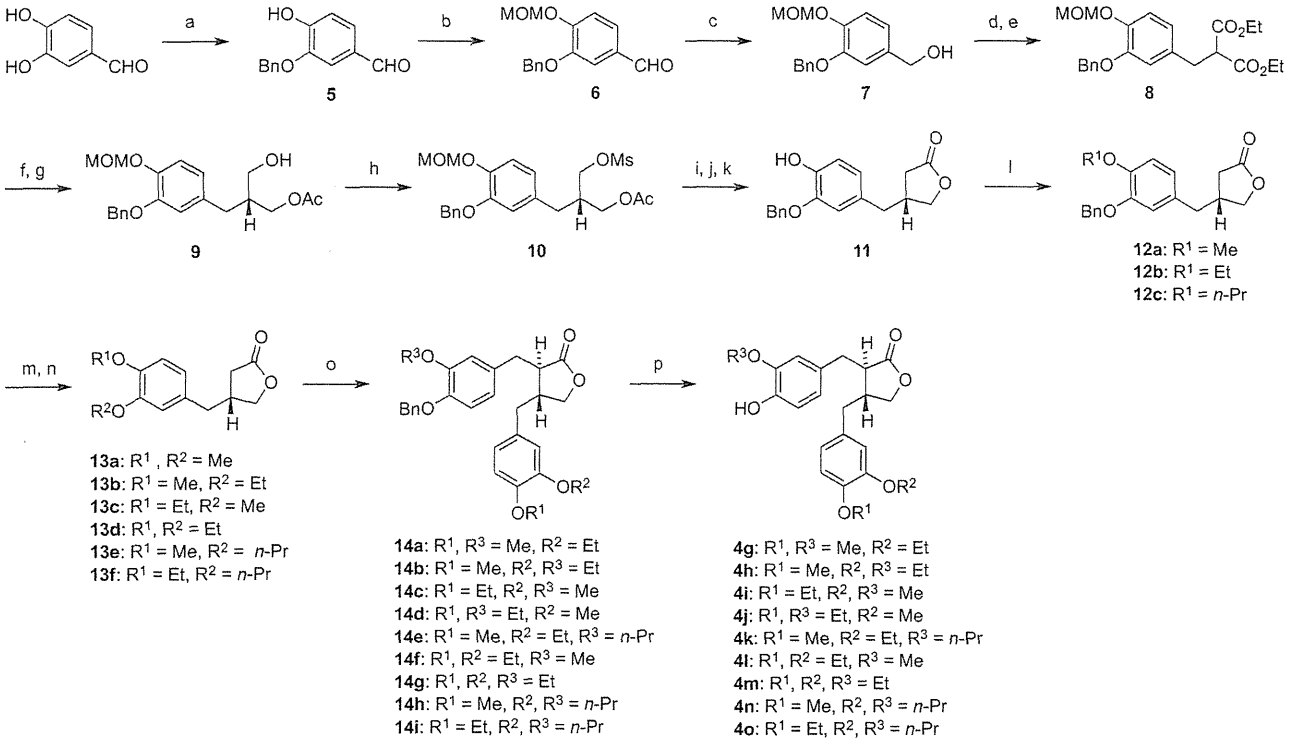

Scheme 2. Reagents and conditions: a: BnBr, K_2CO_3, KI, acetone, reflux (64%); b: MOMCl, DIPEA, CH_2Cl_2, rt (quant.); c: $NaBH_4$, MeOH, rt (95%); d: MsCl, Et_3N, CH_2Cl_2, rt; e: diethyl malonate NaH, DMF, rt (72% in 2 steps); f: $LiAlH_4$, THF, reflux; g: lipase-PS (Amano), vinyl acetate, *i*-Pr_2O–THF rt (80% in 2 steps, 98% ee); h: MsCl, Et_3N, CH_2Cl_2, rt; i: KCN, DMSO, 90 °C; j: LiOH, THF–H_2O, rt; k: 10% NaOH (aq), reflux, then 10% HCl (aq)–THF, rt (73% in 4 steps); l: MeI or EtI or *n*-PrBr, K_2CO_3, acetone, reflux (88% for **12a**, 86% for **12b**, 87% for **12c**); m: H_2, $Pd(OH)_2$, MeOH; *n*: MeI or EtI, K_2CO_3, acetone, reflux (55% in 2 steps for **13a**, 55% in 2 steps for **13b**, 55% in 2 steps for **13c**, 47% in 2 steps for **13d**, 80% in 2 steps for **13e**, 77% in 2 steps for **13f**); o: LiHMDS, substituted BnBr, HMPA, THF, −78 °C to rt (44% for **14a**, 59% for **14b**, 43% for **14c**, 53% for **14d**, 40% for **14e**; 48% for **14f**; 56% for **14g**, 49% for **14h**; 33% for **14i**); p: H_2, $Pd(OH)_2$, MeOH (89% for **4g**, 63% for **4h**, 57% for **4i**, 63% for **4j**, 56% for **4k**, 81% for **4l**, 66% for **4m**, 46% for **4n**, 63% for **4o**).

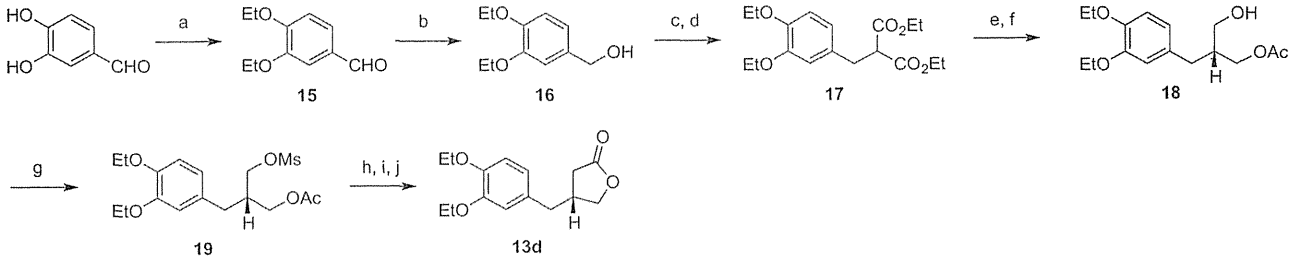

Scheme 3. Reagents and conditions: a: EtI, K_2CO_3, acetone, reflux (92%); b: $NaBH_4$, MeOH, rt (74%); c: MsCl, Et_3N, CH_2Cl_2, rt; d: diethyl malonate NaH, DMF, rt (87% in 2 steps); e: $LiAlH_4$, THF, reflux; f: lipase-PS (Amano), vinyl acetate, *i*-Pr_2O–THF rt (53% in 2 steps, 98% ee); g: MsCl, Et_3N, CH_2Cl_2, rt (79%); h: KCN, DMSO, 90 °C; i: LiOH, THF–H_2O, rt; j: 10% NaOH (aq), reflux, then 10% HCl (aq)-THF, rt (60% in 3 steps).

control group than the groups treated by triethoxy derivative **4m** or (−)-arctigenin (**1**) (Fig. 4C–F). These data indicate that triethoxy derivative **4m** also exerted antitumor activity *in vivo* with the potency identical to or slightly more than (−)-arctigenin (**1**).

3. Conclusion

In summary, a series of new (−)-arctigenin derivatives modified on *O*-alkyl groups were synthesized and their preferential cytotoxicity was evaluated against human pancreatic cancer cell line PANC-1 under nutrient-deprived conditions. The results showed that monoethoxy derivative **4i** (PC_{50}, 0.49 μM), diethoxy derivative **4h** (PC_{50}, 0.66 μM), and triethoxy derivative **4m** (PC_{50}, 0.78 μM) showed the preferential cytotoxicities under nutrient-deprived conditions, which were identical to or more potent than (−)-arctigenin (**1**) (PC_{50}, 0.80 μM). Among them, we selected the triethoxy derivative **4m** and examined *in vivo* antitumor activity with mouse xenograft model. Triethoxy derivative **4m** exhibited also *in vivo* antitumor activity with the potency identical to (−)-arctigenin (**1**). These results would suggest that a modification of (−)-arctigenin structure could lead to a new drug based on the antiausterity strategy.

4. Experimental

4.1. Chemistry

4.1.1. General conditions

Chemicals were purchased from Sigma–Aldrich, Merck, Nakalai Tesque, Wako Pure Chemicals, and Kanto Chemicals, and used without further purification. Column chromatography was done on Cica silica gel 60N (spherical, neutral; particle size, 40–50 μm, Kanto Chemical Co., Inc., Tokyo, Japan), while thin-layer chromatography (TLC) was performed on Merck silica gel $60F_{254}$ plates (Merck KGaA, Darmstadt, Germany). Melting points were taken on a Yanaco micromelting point apparatus and are uncorrected. The nuclear magnetic resonance (NMR) spectra were acquired in the specified solvent, in a Varian Gemini 300 spectrometer (300 and 75 MHz for ^1H and ^{13}C, respectively) or Varian UNITY plus 500 spectrometer (500 and 125 MHz for ^1H and ^{13}C, respectively) (Varian Inc., Palo Alto, CA, USA), with tetramethylsilane (TMS) as internal standard. The chemical shifts (δ) are reported in ppm downfield from TMS and coupling constants (J) are expressed in Hertz. Optical rotations were obtained in the specified solvent on a JASCO DIP-1000 digital polarimeter (JASCO Corp., Tokyo, Japan). IR spectra were measured with a JASCO FT/IR-460 Plus spectrophotometer (JASCO Corp.). The low-resolution mass spectra (MS) and high-resolution mass spectra (HRMS) were obtained with a Shimadzu GCMS-QP 500 mass spectrometer (Shimadzu Corp., Kyoto, Japan), JEOL D-200, or JEOL AX505 mass spectrometer (JEOL Ltd., Tokyo, Japan) in the electron impact mode at the ionization potential of 70 eV.

4.1.2. Synthesis of (−)-arctigenin derivatives *4a–4f*

4.1.2.1. (3R,4R)-3-(4-Benzyloxy-3-hydroxybenzyl)-4-(3,4-dimethoxybenzyl)dihydrofuran-2-one (3). To a stirred solution of (3R,4R)-3-(3,4-dihydroxybenzyl)-4-(3,4-dimethoxybenzyl)dihydrofuran-2-one (**2**) [12] (65.4 mg, 0.18 mmol) in acetone (2 mL) were added K_2CO_3 (37.3 mg, 0.27 mmol), KI (5.97 mg, 0.036 mmol), and BnBr (21.4 μL, 0.18 mmol), and the resulting mixture was refluex for 5 h. After cooling, the reaction mixture was filtered, and the filtrate was evaporated. The residue was chromatographed on silica gel (10 g, hexane:acetone = 4:1) to give **3** (51.2 mg, 63%) as a pale yellow oil: ^1H NMR (300 MHz, $CDCl_3$) δ: 1.60 (1H, br), 2.47–2.63 (4H, m), 2.86–2.98 (2H, m), 3.80 (3H, *s*), 3.85 (3H, *s*), 3.80–3.89 (1H, m), 4.09–4.14 (1H, m), 5.13 (2H, s), 6.47–6.80 (6H, m), 7.28–7.44 (5H, m); ^{13}C NMR (75 MHz, $CDCl_3$) δ: 34.59, 38.19, 41.15, 46.53, 55.82, 55.98, 71.08, 71.21, 111.22, 111.72, 112.79, 113.95, 120.43, 121.20, 127.12, 127.69, 128.39, 130.30, 130.73, 136.98, 146.91, 147.67, 148.84, 149.63, 178.46; IR (neat): 1514 (C=C), 1769 (C=O) cm^{-1}; MS (EI) *m/z* 449 (M^+); HRMS (EI): calcd for $C_{27}H_{28}O_6$: 448.1886 (M^+), found: 448.2743; $[\alpha]_D^{26}$ −20.7 (*c* 0.85, $CHCl_3$).

4.1.2.2. (3R,4R)-4-(3,4-Dimethoxybenzyl)-3-(3-ethoxy-4-hydroxybenzyl)dihydrofuran-2-one (4a). To a stirred solution of **3** (44.7 mg, 0.10 mmol) in acetone (5 mL) were added K_2CO_3 (82.6 mg, 0.60 mmol), EtI (26.5 μL, 0.33 mmol), and the reaction mixture was refluxed for 48 h. After cooling, the reaction mixture was filtered, and the filtrate was evaporated. The residue was dissolved in MeOH (6 mL). To the solution was added 20% $Pd(OH)_2$ (10 mg), and the resulting suspension was stirred under a hydrogen atmosphere at 1 atm for 16 h. The catalyst was removed by filtration and the filtrate was evaporated. The residue was chromatographed on silica gel (7 g, hexane : acetone = 3:1) to give **4a** (13.4 mg, 35% in 2 steps) as a colorless oil: ^1H NMR (300 MHz, $CDCl_3$) δ: 1.41 (3H, t, J = 7.1 Hz), 2.42–2.64 (4H, m), 2.90 (2H, d, J = 5.2 Hz), 3.80 (3H, s), 3.84 (3H, s), 3.80–3.88 (1H, m), 4.02 (2H, q, J = 7.1 Hz), 4.08–4.13 (1H, m), 5.66 (1H, br), 6.46–6.75 (4H, m), 6.81 (1H, d, J = 8.0 Hz); ^{13}C NMR (75 MHz, $CDCl_3$) δ: 14.85, 30.94, 34.48, 38.15, 40.90, 46.58, 55.85, 64.38, 71.24, 111.11, 111.61, 112.29, 113.94, 120.43, 121.83, 129.20, 130.30, 144.47, 145.80, 147.62, 148.81, 178.51; IR (neat): 1516 (C=C), 1766 (C=O), 3446 (OH) cm^{-1}; MS (EI) *m/z* 386 (M^+); HRMS (EI): calcd for $C_{22}H_{26}O_6$: 386.1729 (M^+), found: 386.1724; $[\alpha]_D^{26}$ −20.5 (*c* 0.98, $CHCl_3$).

4.1.2.3. (3R,4R)-4-(3,4-Dimethoxybenzyl)-3-(4-hydroxy-3-propoxybenzyl)dihydrofuran-2-one (4b). By the procedure similar to synthesis of **4a**, (−)-arctigenin derivative **4b** was prepared from **3** and *n*-PrBr (18% in 2 steps) as a colorless oil: ^1H NMR (300 MHz, $CDCl_3$) δ: 1.04 (3H, t, J = 1.9 Hz), 1.77–1.87 (2H, m), 2.42–2.67 (4H, m), 2.81–3.01 (2H, m), 3.78–3.86 (7H, m), 3.90–4.00 (2H, m), 4.09–4.14 (1H, m), 5.59–5.63 (1H, br), 6.47–6.85 (6H, m); ^{13}C NMR (75 MHz, $CDCl_3$) δ: 10.60, 22.60, 29.34, 31.81, 34.55, 38.22, 41.49, 46.65, 53.80, 55.82, 70.35, 71.29, 111.71, 113.94, 115.27, 120.47, 121.85, 112.34, 129.28,